Transient x-ray diffraction from polycrystalline beryllium

Damian C. Swift,*

P-24 Plasma Physics

Los Alamos National Laboratory, †Los Alamos, NM 87545, USA

LA-UR-04-8534 – November 19, 2004

Abstract

Diffraction lines were obtained from samples of beryllium foil using pulses of collimated x-rays as short as 1 ns in duration. This diagnostic is the analog of the single crystal diffraction measurements made previously using uncollimated x-rays, to coincide with shock compression of the sample by laser ablation. Equivalent experiments were made with polycrystalline samples, to demonstrate that shock compression could be observed in dynamic powder diffraction. This was a somewhat favorable case in terms of signal: the samples were rolled foils, with many of the grains oriented preferentially around the direction in which signals would be obtained for zero and low shock compressions; on the other hand, beryllium was a disadvantageous material in that the scattering efficiency for x-rays was relatively low. Diffraction signals were observed on time-integrating films and also on time-resolving x-ray streak cameras, and in transmission as well as reflection. Some of the streak records may have exhibited spurious lines from camera problems. The diffraction angles deduced were consistent with uniaxial (elastic) and isotropic (plastic) compressions expected for the loading conditions used.

*dswift@lanl.gov

†This work was performed under the auspices of the U.S. Department of Energy under contract # W-7405-ENG-36.

Contents

1 Introduction

Shock wave experiments are a standard way of investigating the high pressure behavior of materials [1], particularly for developing models of the response of materials to dynamic loading such as shocks themselves. The usual experimental measurements, developed on facilities such as projectile impacts, include the speed of the shock wave and the material speed behind the shock. More recently, measurements have been made of other properties of the shocked material, such as the deformation of the crystal lattice through *in situ* x-ray diffraction [2, 3, 4, 5], known by various names including 'transient x-ray diffraction' (TXD). These experiments are challenging in synchronizing the x-rays with the shock, and in the short duration of the event which makes it difficult to obtain adequate signal levels in the diffraction lines. Previous experiments have reported diffraction lines from individual crystals. TXD data are potentially extremely valuable as direct measurements of the elastic compression of the crystal lattice, the onset of plastic flow, phase transitions, and the density of crystal defects such as dislocations.

TXD data from polycrystalline samples are desirable in several respects. Using a single crystal, the point at which diffraction occurs moves across the sample as the lattice spacing changes. For high compressions, it can be difficult to ensure that both the unshocked and shocked lines can be accommodated over the finite width of the shocked region (Fig. 1). In contrast, polycrystalline diffraction is best arranged from a single point (or small area) of the sample, and does not move with compression. Another compelling reason is that, for many materials, polycrystalline samples are far easier to obtain.

We have performed TXD experiments on single crystals of a variety of materials, notably beryllium [6]. Beryllium-based alloys are of technological interest as the deuterium-tritium fuel capsule for inertial confinement fusion (ICF) [7, 8, 9]. Experiments on beryllium are intended to investigate the anisotropy of plastic response under dynamic loading, and phase transitions including melting. As well as their technological significance, TXD data from these experiments are valuable in understanding plasticity in hexagonal metals and the dynamics of melting. Shock loading was induced by laser ablation (Fig. 2): the loading history is often less simple and less well-characterized than is the case for projectile impact experiments, but laser-induced shocks are far easier to synchronize with laser-powered x-ray sources, and are more appropriate for the length and time scales of interest for ICF: $\sim 100\,\mu$m and 1 ns. Recently, we have developed a reasonably accurate predictive capability to relate the pressure history of the shock to the irradiance history of the laser pulse [10, 11]; radiation hydrodynamics simulations can be used to understand the loading history, and to adjust the temporal structure of the pulse to induce a constant drive pressure and hence a better-characterized shock.

The single crystal beryllium TXD experiments fired previously used the only material to hand at the time: samples cut parallel to (0001) planes, and with a rocking curve around 2° wide: far from a perfect crystal. The experiments described here were part of a series performed to evaluate whether polycrystal diffraction could supplement the single crystal experiments on beryllium, reducing the need for further difficult-to-obtain crystals. These experiments were performed at the TRIDENT laser facility during a series in July-August 2001 [12], and also during the 'Flying Pig 2' series in August 2002 [13]. For completeness, this report contains all records showing a measurable signal, including some likely to suffer from camera faults.

2 Laser ablation experiments

Each sample was loaded by irradiation using the TRIDENT laser; pressure was generated by ablation of material from one surface (Fig. 2). The velocity history of the opposite surface (across the thin direction) was measured using line-imaging Doppler velocimetry. X-rays were generated by irradiating a thin metal foil with a second laser pulse, tightly-focused, to produce a hot plasma. The resulting x-rays were collimated to illuminate the target with a narrow beam. This was diffracted from the sample and recorded using film and an x-ray streak camera as a measure of the lattice compression. (Fig. 3.)

2.1 Sample material

Beryllium foils were obtained from Goodfellow Inc, of 99.8% purity (the maximum supplied). These were rolled foils, with significant texture. The texture was investigated by obtaining x-ray orientation maps of a

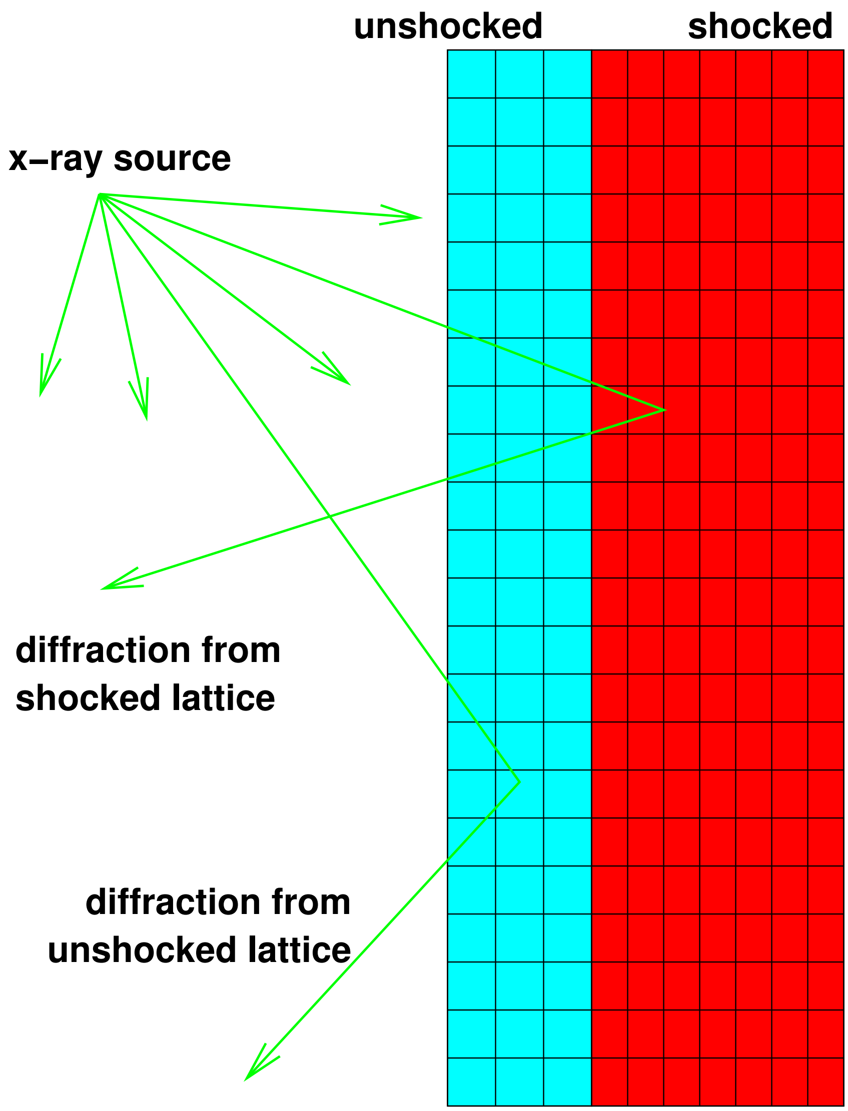

Figure 1: Schematic of transient x-ray diffraction from a single crystal sample, illustrating diffraction from different points at different compressions.

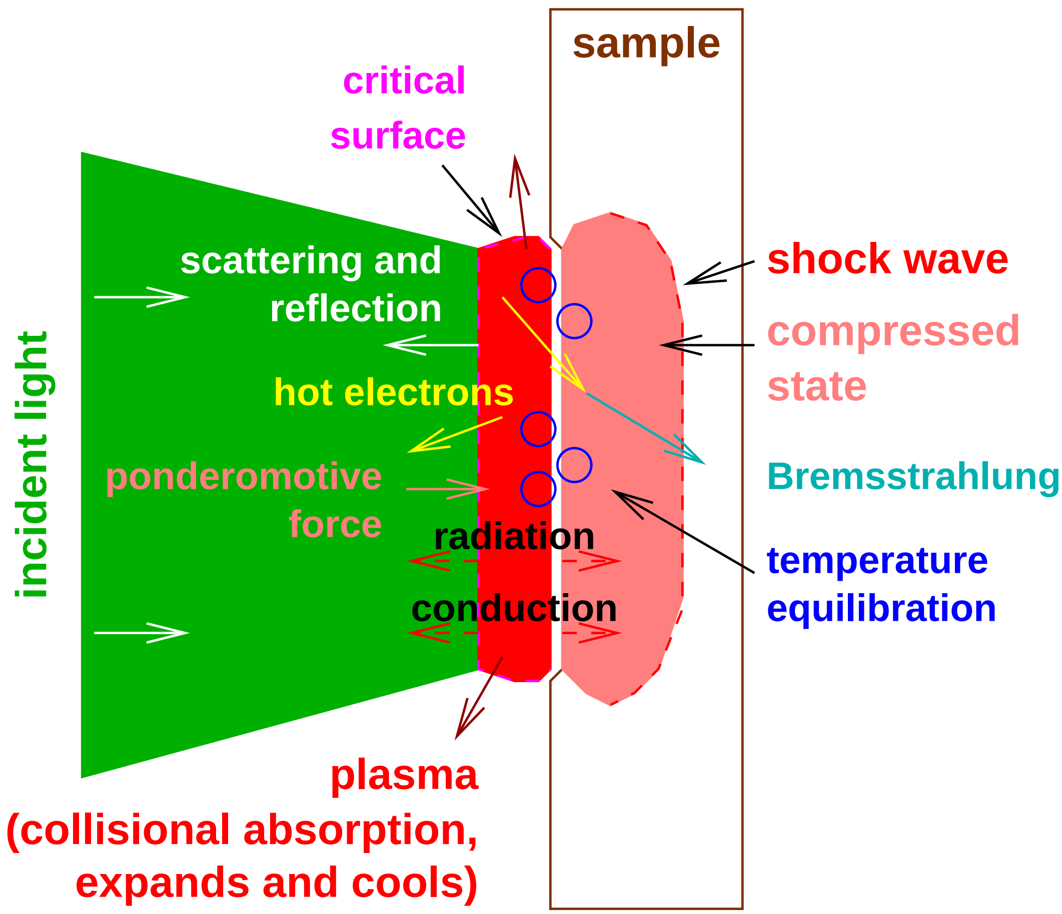

Figure 2: Schematic of shock generation by laser ablation.

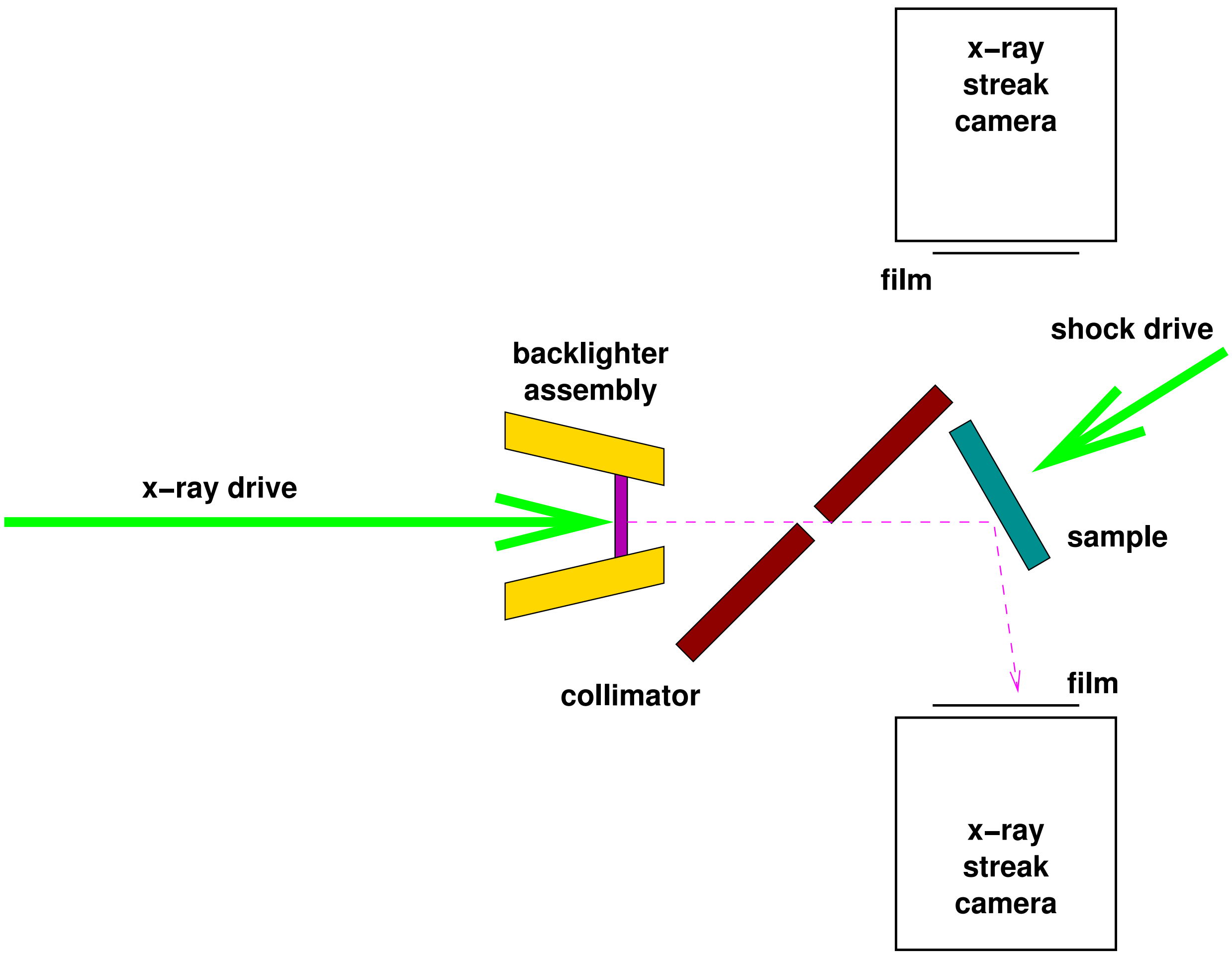

Figure 3: Schematic of experimental layout (not to scale).

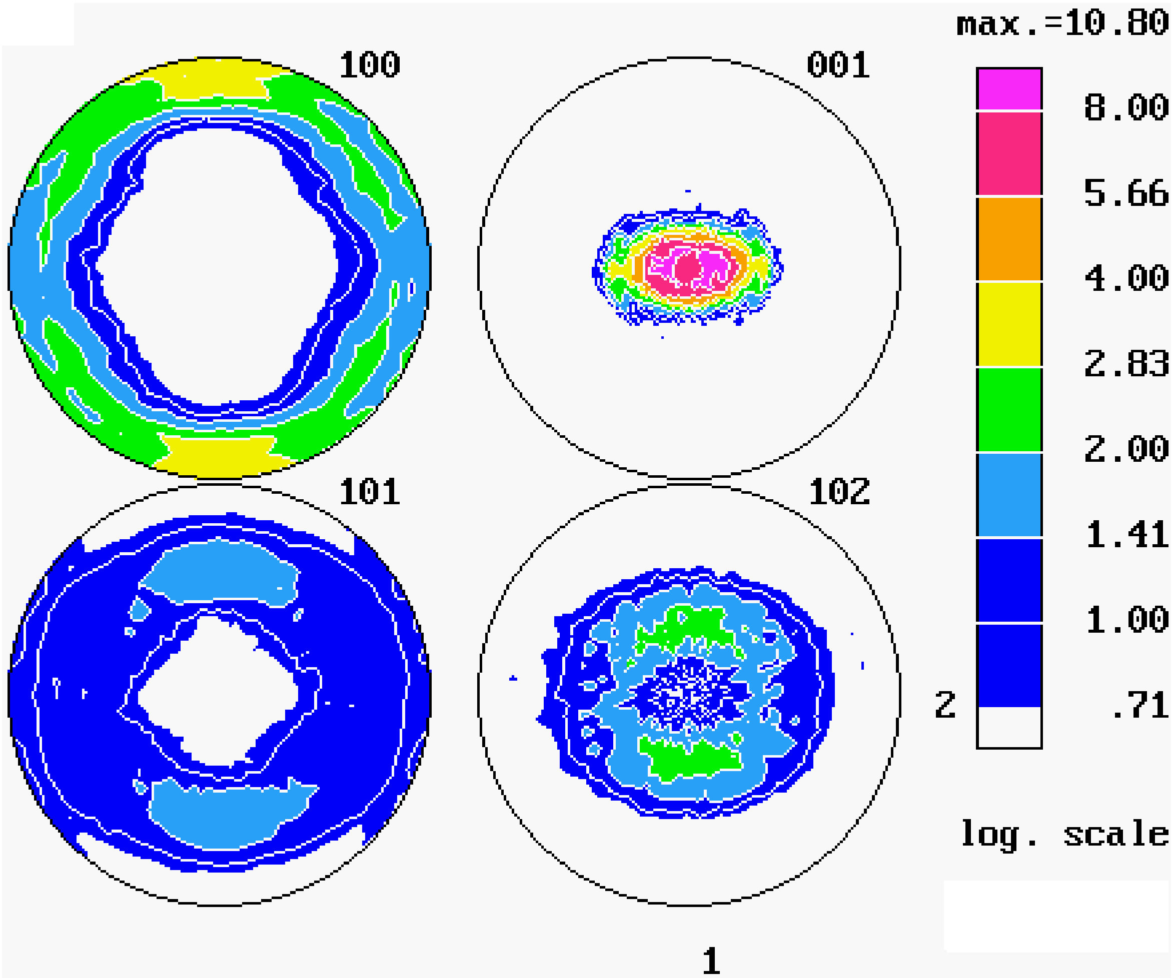

Figure 4: Orientation maps of crystal planes in foils 125 μm thick. Each circular figure is a stereographic projection, showing a colormap of the distribution of normals to one plane. The center of the circle is the normal to the sample; the circumference is the set of directions lying in the plane of the sample.

couple of sample foils. The scattering efficiency of beryllium is low, so the thicker foils (125 μm) were used in these measurements. The foils were found to be oriented preferentially so that normals to the (0001) planes were distributed around the normal to the foil, equivalent to a rocking curve a couple of tens of degrees wide. The $(10\bar{1}0)$ planes were distributed with normals in the plane of the sample, though with significant variation in this azimuthal distribution – presumably a memory of the directions in which the foil was rolled. (Fig. 4.)

If the grains in the sample were oriented isotropically, the powder diffraction pattern obtained with x-rays of the wavelength used in these experiments would comprise a cluster of three lines within 10° of 90° from straight through the sample, which is roughly the area covered by the x-ray diagnostics. (Figs 5 and 6.)

2.2 Target assembly

A re-usable holder was used to locate the sample and x-ray source for each shot (Fig. 7). The sample assembly was clamped by the edges, the holder having apertures for the drive and velocimetry beams. The holder was designed for use with a wide sample assembly, i.e. a large aperture for the sample, so that the clamp-type arrangement used to hold the sample would be well out of the region illuminated by the x-rays and thus unlikely to increase the x-ray background by fluorescence. Thus either a wide sample was needed

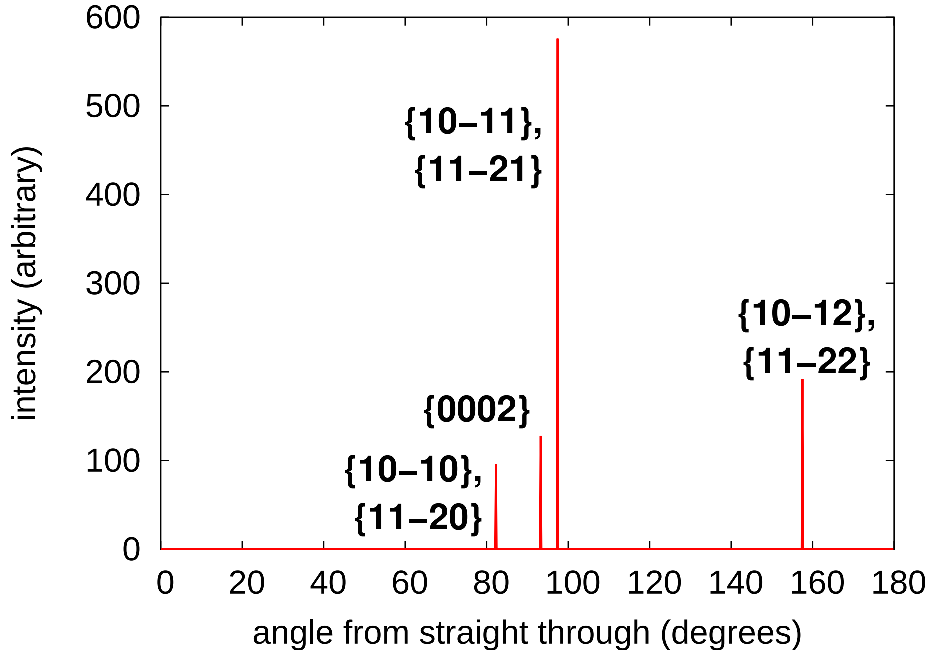

Figure 5: Simulated powder pattern for polycrystalline beryllium.

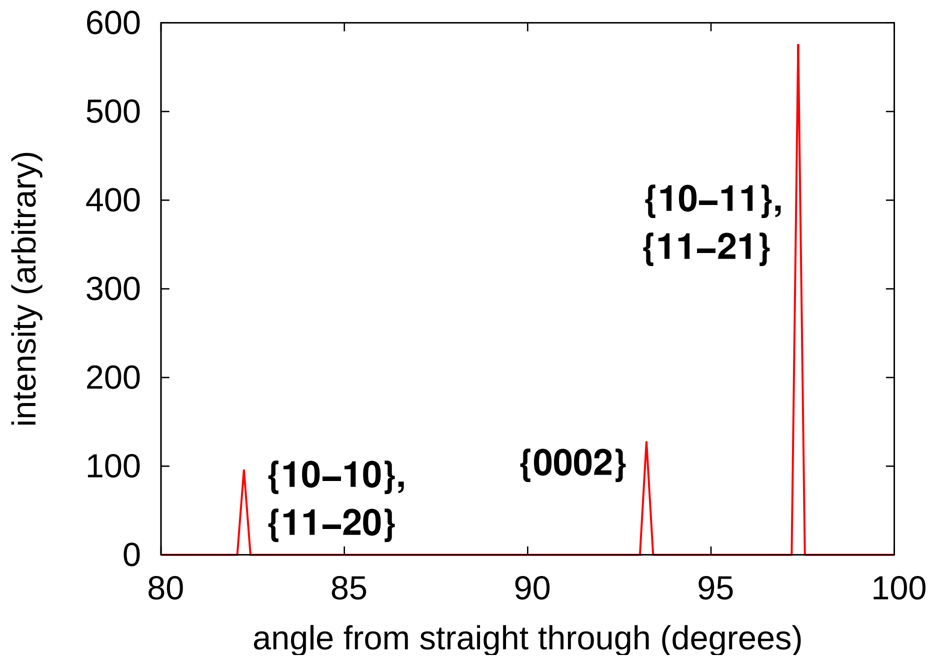

Figure 6: Simulated powder pattern for polycrystalline beryllium (range of angles captured by detectors).

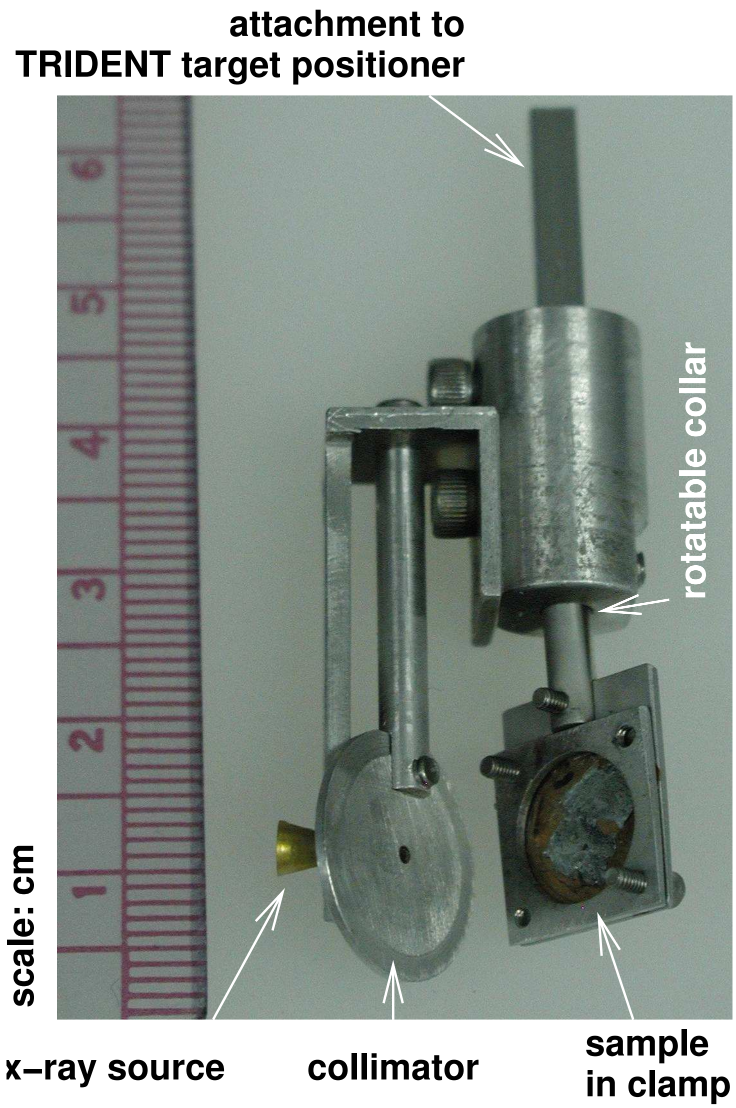

Figure 7: Re-usable clamp-type target holder ('Ortiz holder').

(∼10 mm across), or the sample was attached to a retaining mount (e.g. a washer) of a material which would not cause problems with x-ray fluorescence. For the beryllium experiments, pieces were cut which were large enough to fill the full aperture in the holder.

2.3 Diagnostics

Because of the design of the nose of the x-ray streak cameras, x-ray diffraction was the only diagnostic possible of the shocked state in these experiments. Ablative loading experiments were performed on beryllium foils previously, with surface velocimetry but no diffraction [14, 15] The temporal shape of the laser drive pulse was also measured, and used in conjunction with radiation hydrodynamics simulations to calculate the loading history applied to each sample.

In situ x-ray diffraction was performed using a collimated plasma backlighter as the x-ray source, with Bragg diffraction from the opposite side of the sample as the ablation drive. Diffraction lines were recorded on DEF film (time-integrating) and using a Kentech x-ray streak camera.

The plasma backlighter used the A beam of TRIDENT, focused tightly (∼150 μm diameter spot) on a metal foil $\sim$10 μm thick to generate a hot plasma which emitted essentially monochromatic radiation. The A and B beams were driven from the same master oscillator, so they shared the same duration and un-amplified pulse shape, though the energies were controlled independently. The pulse shape was chosen to optimize the shock drive (see below); the energy was chosen to excite atoms in the plasma to a helium-like state (fully ionized except for two electrons). The x-ray wavelength was controlled through the choice of backlighter material: in this case titanium for 2.61 Å (4.75 keV). The backlighter was mounted inside a truncated gold cone, which prevented direct irradiation of the diffraction diagnostics by the source. The emission spectrum was recorded using a transmission grating.

The plasma source emitted x-rays roughly isotropically into 4π steradians. For diffraction from a polycrystalline sample, it is necessary to use a collimated source. An aluminum disk, 1 mm thick and 15 mm in diameter, was used as the collimator. A hole 1 mm in diameter was drilled through the center to define the beam size. This rather large size was chosen so that a signal would be more likely to be observed in early trials. The collimator was twisted with respect to the x-ray axis in subsequent experiments to present a narrower (non-circular) aperture.

X-rays from the plasma were incident on the sample material, and diffracted from individual grains according to the Bragg condition. The attenuation length of $\sim$5 keV x-rays in beryllium is several hundred microns, compared with sample thicknesses of a few tens of microns. Thus the diffraction signals were averages through the entire thickness of each sample, in general comprising material in different states of compression. If compressed material was present – e.g. behind the shock wave – during the backlighter pulse, the x-rays were diffracted at a different angle. The timing of the x-rays was altered with respect to the shock drive, by changing the path length of the backlighter beam using a manual trombone. Typical delays were $\sim$2 ns.

The slit of the x-ray streak camera was horizontal and the samples were mounted as vertical planes. Each slit subtended an angle of 12° at the target. The time-integrating film subtended an angle of 20° – constrained by the inside diameter of the cylindrical camera snout.

Filter foils were added in front of the film pack, or between the film pack and the photocathode of the x-ray streak camera, to control the signal level. 125 μm of beryllium was used in all cases, with $\sim$25 μm of titanium, adjusted for best signal.

The energy in the backlighter beam was typically 150 to 200 J over 1.0 ns for a titanium backlighter.

The x-ray streak cameras were attached to the north and south chamber ports. The Bragg angles of unshocked material were used to select the appropriate backlighter material: titanium for use with beryllium at low compressions. The orientation of the experiment was chosen so that {0001} would be within the field of view of the detectors in the south port.

It was possible for signals to be observed on the x-ray streak cameras but not on the time-integrating films placed in front of the cameras, because the cameras were much more sensitive than the film. The light signal from the streak tube was amplified with an image intensifier before recording on optical film (TMAX).

2.4 Drive beam

TRIDENT was operated in nanosecond mode, in which each pulse comprises up to 13 consecutive elements whose intensity can be controlled separately. Using all elements, the drive pulse would be 2.5 ns long. For the TXD experiments reported here, the pulse length was shorter (fewer elements used) to optimize the efficiency of energy conversion to x-rays. The pulses generated were approximately square, usually with a slight ramp with the intention of generating a more constant pressure. The fundamental light from the laser was frequency-doubled to 527 nm, and focused through a Fresnel zone plate to produce roughly uniform irradiance over a spot 5 mm in diameter. The pulse energy and intensity history were recorded on each shot.

3 Loading histories

Surface velocimetry has been used as the primary diagnostic for inferring the loading history applied to the sample, by identifying the amplitude of any elastic precursor wave and of the plastic shock and by constraining simulations of the loading applied by the laser drive. Surface velocities were not recorded on the experiments described here, because of conflicts with the position of the x-ray detectors. However, extensive studies of shock loading of beryllium foils were performed previously [14], giving confidence in the accuracy of simulations.

3.1 Radiation hydrodynamics

Radiation hydrodynamics simulations were used to simulate the loading history induced by laser ablation. Depending on the time scales and irradiance, many physical processes may need to be included to reproduce laser-matter interactions accurately. However, in the regime explored by these experiments (picosecond to nanosecond time scales, laser irradiance $\sim$0.1 to 10 PW/m^2), previous experience using the LASNEX radiation hydrocode [16] suggested that laser ablation and dynamic loading could be simulated accurately by assuming three temperature hydrodynamics (ions, electrons, and radiation), allowing thermal conduction and radiation diffusion, and calculating the absorption of the laser energy in the expanding plasma cloud through the electrical conductivity. This model was needed only for material ablated by the laser: a region $\sim$1 μm wide of the solid sample, and the resulting plasma cloud. The remainder of the condensed phase could be treated using non-radiative continuum mechanics, i.e. with an equation of state (EOS) and, optionally, a constitutive model. Some specific processes excluded in this plasma model include resonant absorption, transport of the resulting hot electrons, and generation, transport, and deposition of Bremsstrahlung x-rays.

Simulations were performed using the HYADES radiation hydrocode, version 01.05.11 [17]. This hydrocode used a 1D Lagrangian discretization of the material, and leapfrog time integration, and did not include material strength in the solid sample. Shock waves were stabilized using artificial viscosity. The EOS and opacity were represented using tabular models from the SESAME database [18]. Conductivities for laser deposition and heat conduction were calculated using the Thomas-Fermi ionization model [17, 19]; this was found previously to be reasonably accurate for direct drive shock simulations on samples of a wide range of atomic numbers [10]. The flux limiter was set to 0.03 of the free stream value - a common choice for simulations of this type [20].

The initial spatial mesh was set up to be expanding, to allow adequate resolution of the material to be ablated. Moving away from the sample surface, adjacent cells were expanded by 5%. The cell closest to the surface was 5 nm wide. Previous sensitivity studies had demonstrated that this resolution was adequate for direct drive simulations in this regime of irradiance and time scale [10]. Where possible, simulations were performed using the irradiance history measured on each shots to infer the precise loading history applied to each sample. The exceptions were experiments in which the photodiode measuring drive history was saturated; in these cases, the shape was assumed to be the same as for shots fired shortly before or after, and the amplitude was scaled to give the correct total energy. The raw photodiode record was converted to irradiance by scaling so that the integral under the curve matched the measured pulse energy, and dividing by the area of the focal spot. The raw record contained high frequency fluctuations, giving negative apparent values of the irradiance when the signal was low. For the simulations, the inferred irradiance history was reduced to a piecewise linear variation reproducing the principal features to a few percent in irradiance.

3.2 Continuum mechanics

Continuum mechanics simulations were used to predict the propagation and evolution of the loading history through the thickness of the sample, taking account of the constitutive properties (elasticity and strength) of the material. Simulations were performed using the LAGC1D hydrocode, version 5.2 [21]. This hydrocode used a 1D Lagrangian discretization of the material, and predictor-corrector time integration. Shock waves were stabilized using artificial viscosity.

Table 1: Laser ablation experiments on beryllium foils with x-ray diffraction.

shot	**sample thickness** (μm)	**pulse duration** (ns)	**drive energy** (J)	**backlighter energy** (J)	**comments**
13655	125	1.8	63	261	no TXD data
13657	125	1.8	150	178	
13662	125	1.8	0	241	static TXD test
13664	125	1.8	0	235	static TXD test
13673	25	1.8	0	147	static test; no TXD data
13674	25	1.8	0	103	static test; no TXD data
15000	25	1.0	0	145	static TXD test
15002	55	1.0	50	209	
15004	25	1.0	0	179	static TXD test
15009	55	1.0	49	208	
15012	55	1.0	103	198	
15014	55	1.0	115	168	
15024	55	1.0	222	209	

4 Results

Six experiments were performed in 2001, and seven in 2002 (Table 1). In all cases, the sample was a rolled foil of beryllium, and the backlighter was titanium. For the pulses 1.0 ns long, TRIDENT supplied elements 8 through 13. For the 1.8 ns pulses, elements 5 through 13 were used.

The drive energy was measured with a calorimeter, and the irradiance history of the drive pulse with a photodiode. The uncertainty in energy was of the order of 1 J. In some experiments, the filtering was incorrect and the photodiode signal was saturated. No signal was recorded during saturation, so the irradiance during the non-saturated parts of the record were typically scaled by too great a value to give the correct total energy. For saturated records, radiation hydrodynamics were performed using estimates of the irradiance history based on the requested pulse shape and also by scaling the shape measured on shots performed at a similar time.

On some the earlier experiments, no TXD data were obtained (as opposed to data on the source spectrum) because of incorrect filtering. These experiments are not considered further here.

4.1 13657

In shot 13657, the filtering was inadequate on the photodiode monitoring the drive beam, so the pulse shape record was saturated around its peak. The collimator plane was close to normal to the desired x-ray axis, giving a large spot size on the sample. Neither of the time-integrated films, nor the Bragg time-resolved record, showed any signal. The time-resolved Laue record showed two broad lines. (Figs 8 and 11.)

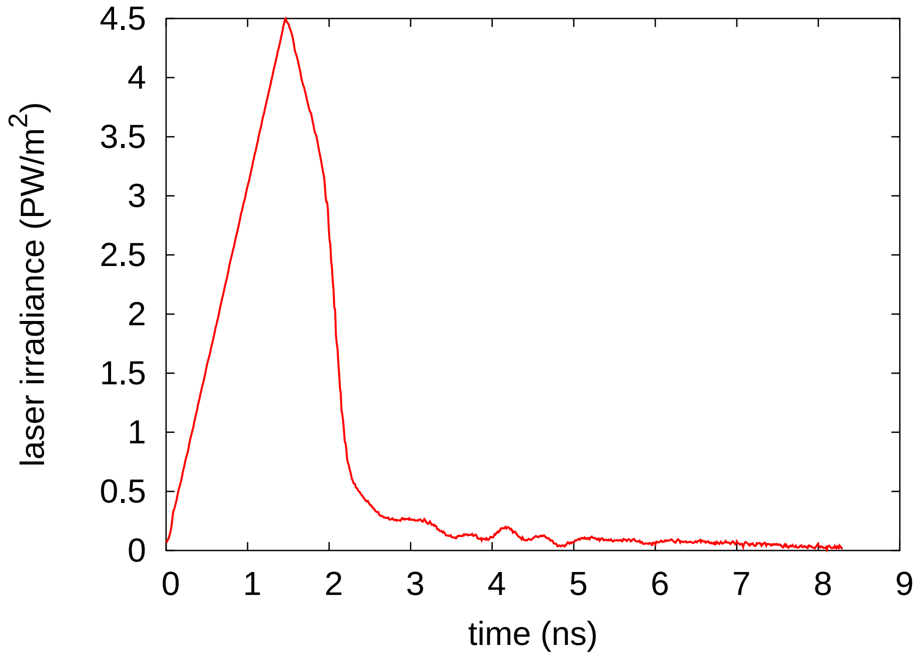

Figure 8: Laser irradiance history, shot 13657.

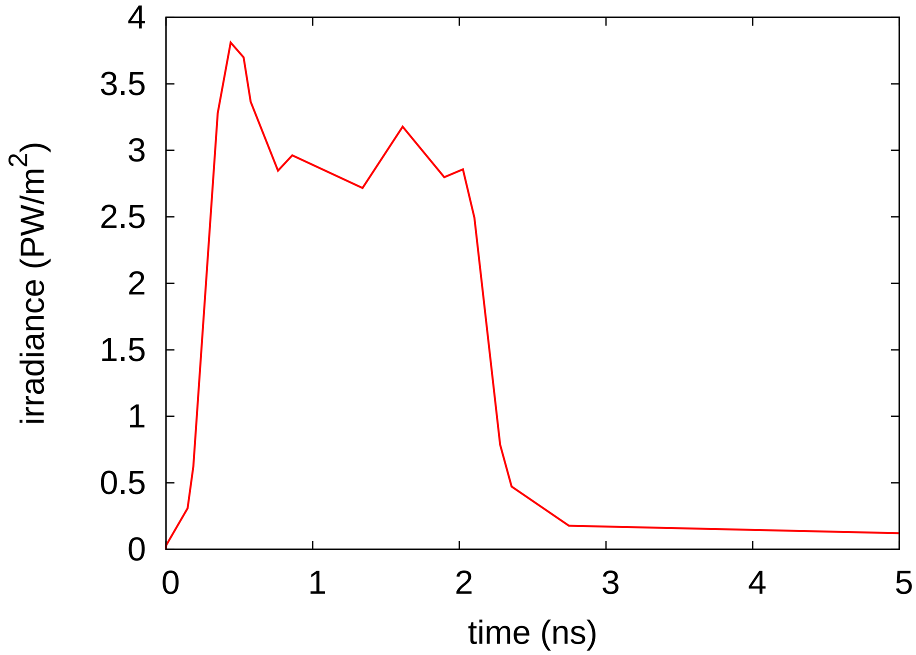

Figure 9: Laser irradiance history used for simulations of shot 13657.

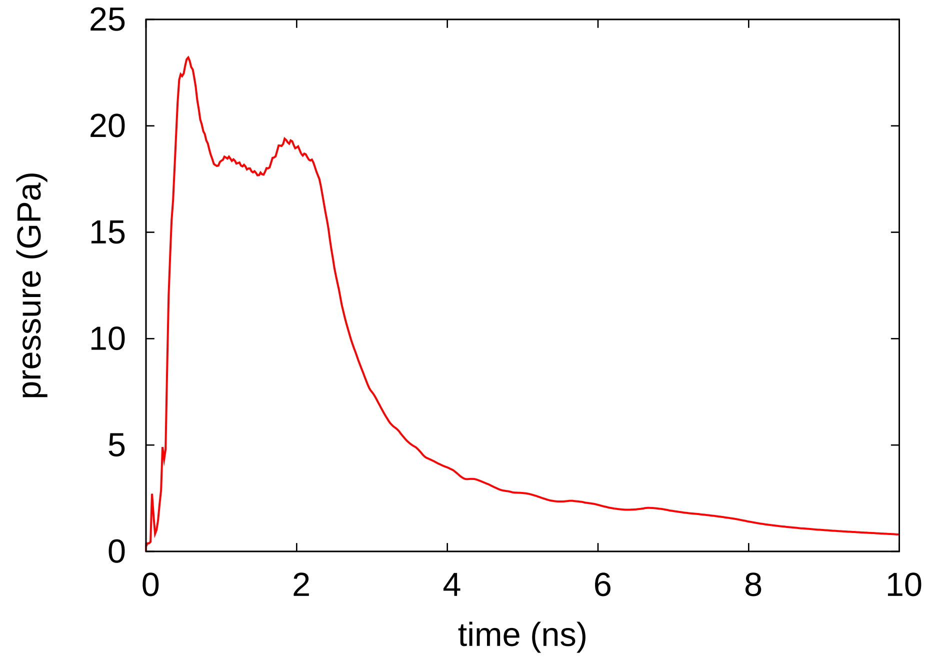

Figure 10: Drive pressure history predicted from radiation hydrodynamics simulations, shot 13657.

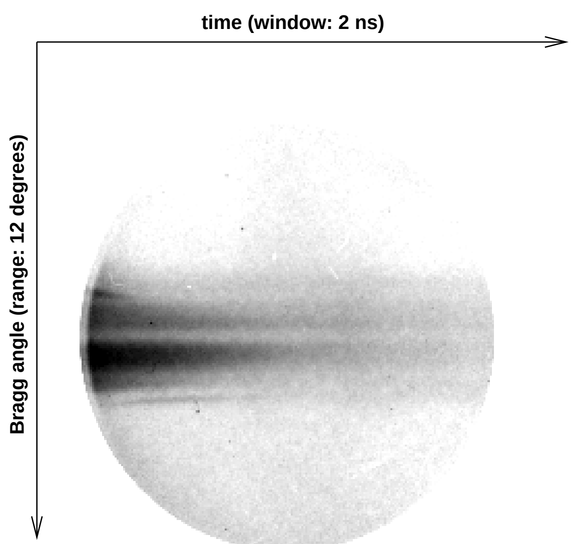

Figure 11: Time-resolved Laue diffraction record, shot 13657.

4.2 13662

Shot 13662 was a static test of x-ray diffraction, with different filtering to the previous experiment. The time-integrated Bragg film was saturated; the Laue film showed no signal. The time-resolved Bragg record showed two pairs of lines; each pair resembling the doublet structure previously observed from the x-ray source during experiments on silicon crystals [5]. This record also showed rectangular regions of greater exposure – this may be a symptom of problems with the camera sweep timing. The time-resolved Laue record showed at least two lines. (Figs 12 to 14.)

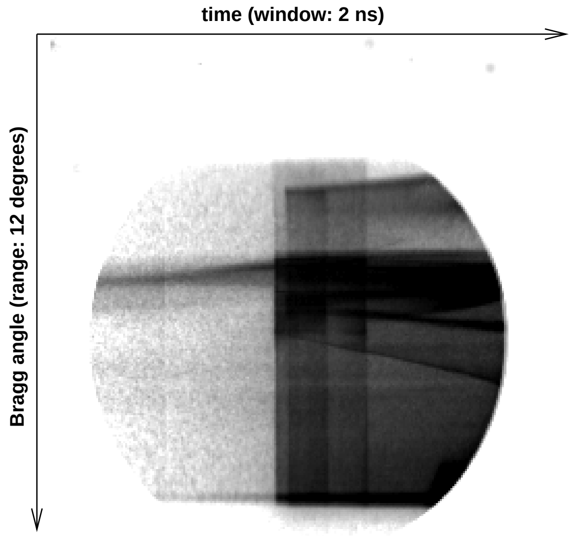

Figure 12: Time-resolved Bragg diffraction record, shot 13662.

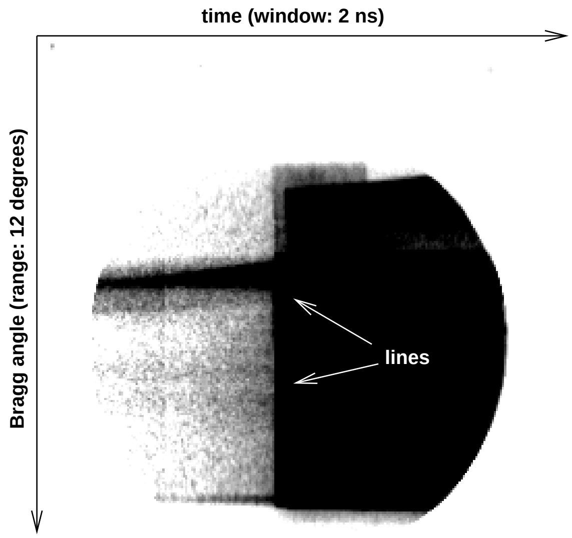

Figure 13: Time-resolved Bragg diffraction record, shot 13662 (modified greyscale limits).

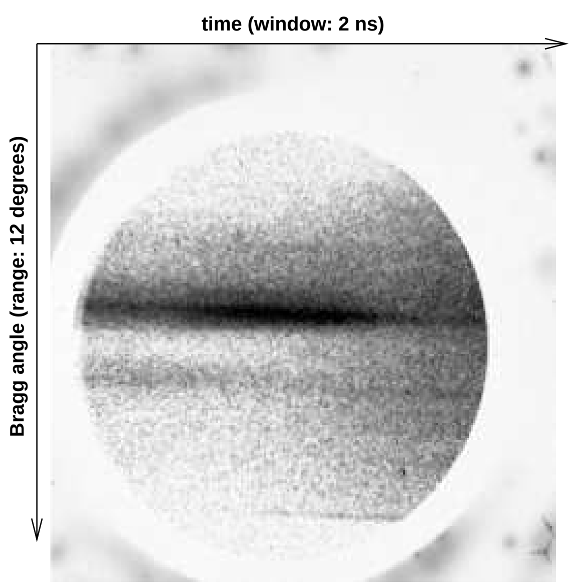

Figure 14: Time-resolved Laue diffraction record, shot 13662.

4.3 13664

Shot 13664 was a static test of x-ray diffraction, with different filtering to the previous experiment. The time-integrated Laue film was saturated; the Bragg film showed no signal. The time-resolved Bragg record again showed two pairs of lines. Again, there were rectangular regions of greater exposure, a possible symptom of problems with the camera sweep timing. The time-resolved Laue record showed at least two lines. (Figs 15 and 16.)

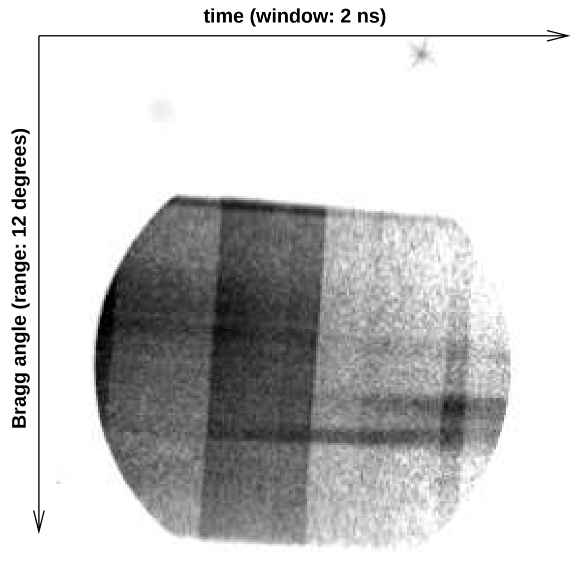

Figure 15: Time-resolved Bragg diffraction record, shot 13664.

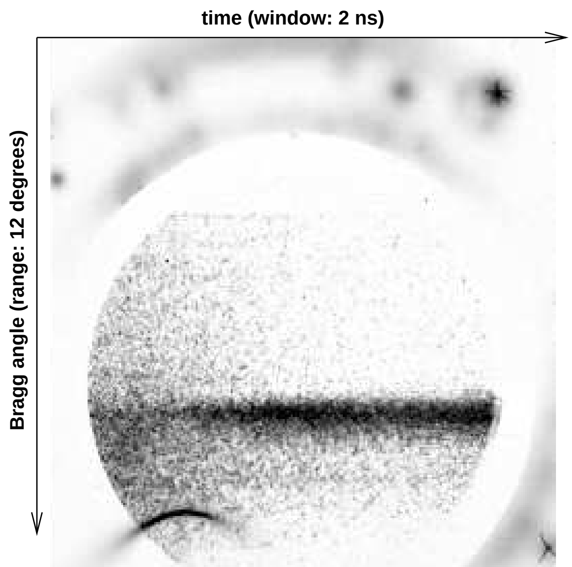

Figure 16: Time-resolved Laue diffraction record, shot 13664.

4.4 15000

Shot 15000 was a static test of x-ray diffraction: the backlighter beam was fired but not the drive beam. The collimator plane was normal to the desired x-ray axis, giving the largest spot size on the sample, nominally 8° at the camera. The streak camera record showed a broad line, consistent with the collimator setting. (Fig. 17.)

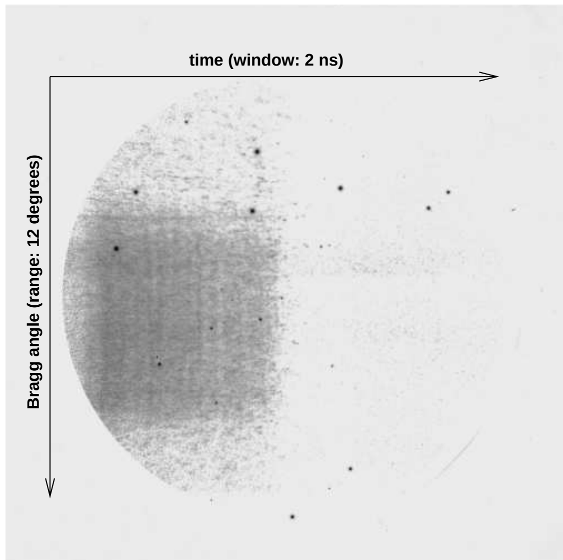

Figure 17: Time-resolved Bragg diffraction record, shot 15000.

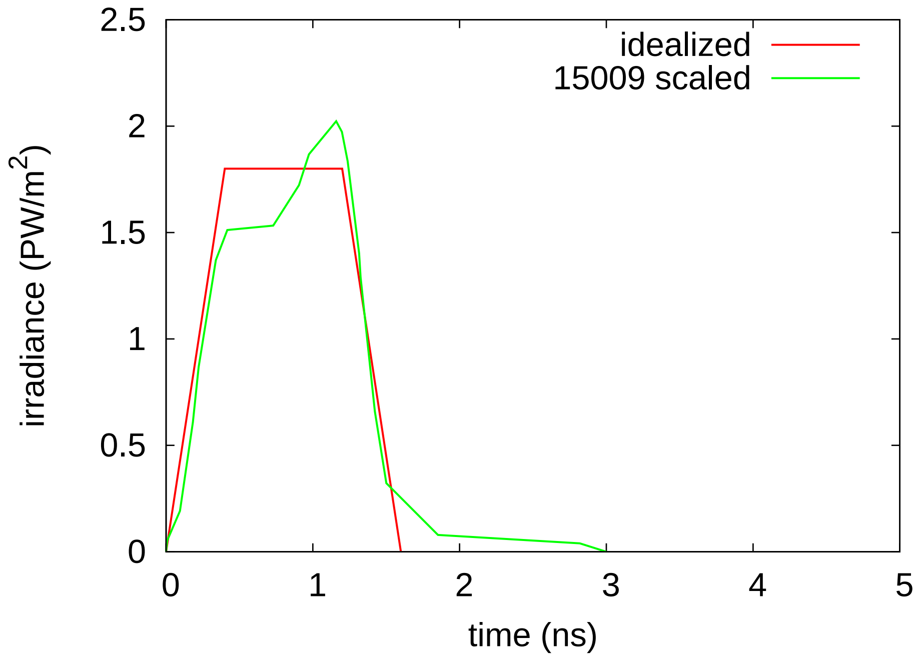

Figure 18: Laser irradiance history used for simulations of shot 15002.

4.5 15002

From shot 15002, the collimator disk was twisted to present a smaller aperture to the x-rays. The filtering was inadequate on the photodiode monitoring the drive beam, so the pulse shape record was saturated. Simulations were performed using two drive histories: an idealized pulse based on the requested shape, and an energy scaling of the pulse obtained in shot 15009. The time-integrated Bragg record showed a broad, curved line with a mottled intensity; the mottling may be caused by reflections from individual crystals of different size. The time-resolved Bragg record showed two clear lines: one narrow with a suggestion of a doublet structure, likely the unshocked signal, and one broad and with shorter duration, likely from shocked material with a significant variation in compression. The time-integrated Laue record was slightly exposed at the edges, suggesting lines just out of the field of view. There was no signal on the time-resolved Laue camera. (Figs 18 to 22.)

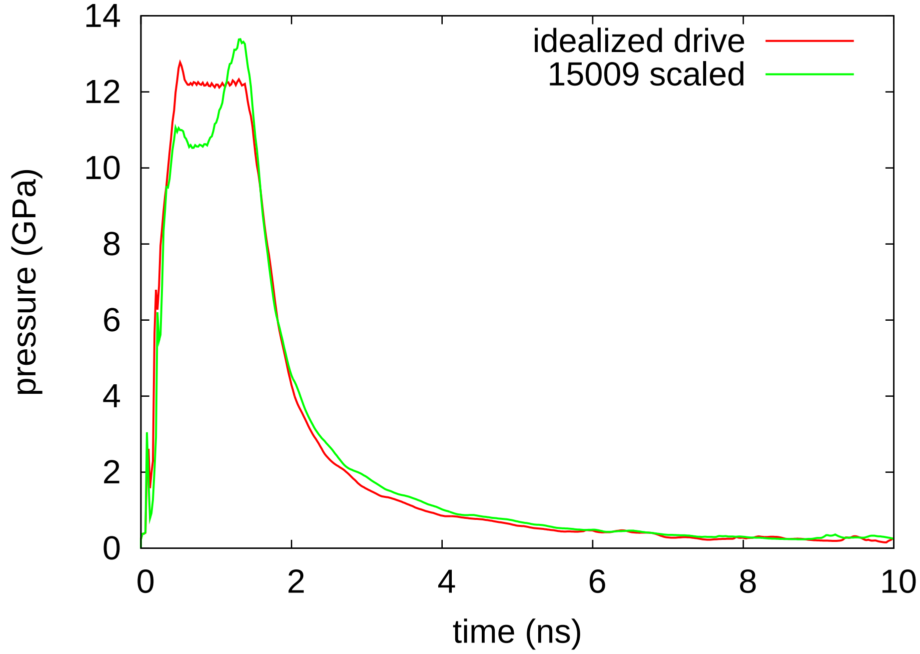

Figure 19: Drive pressure history predicted from radiation hydrodynamics simulations, shot 15002.

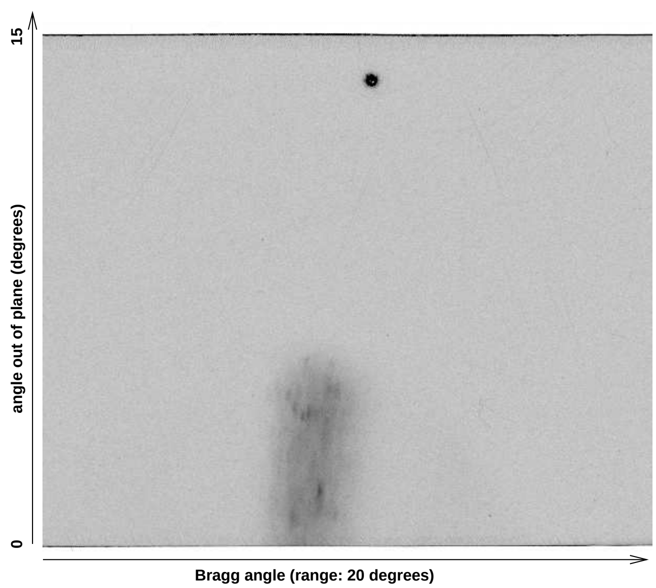

Figure 20: Time-integrated Bragg diffraction record, shot 15002.

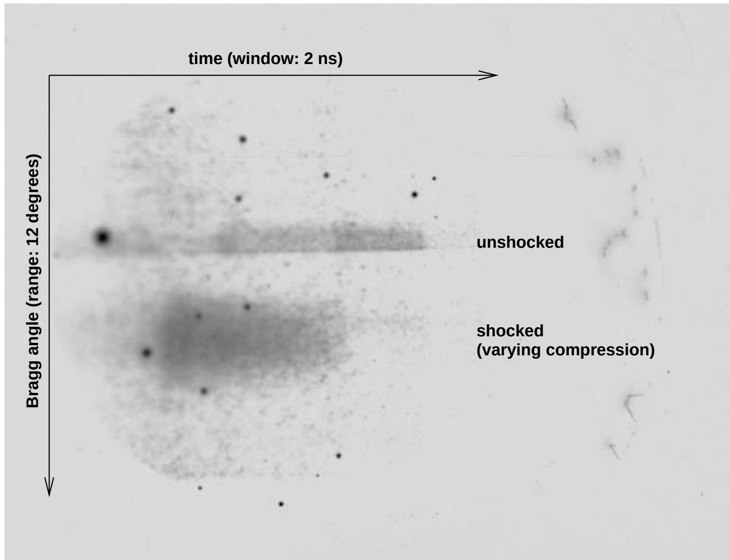

Figure 21: Time-resolved Bragg diffraction record, shot 15002.

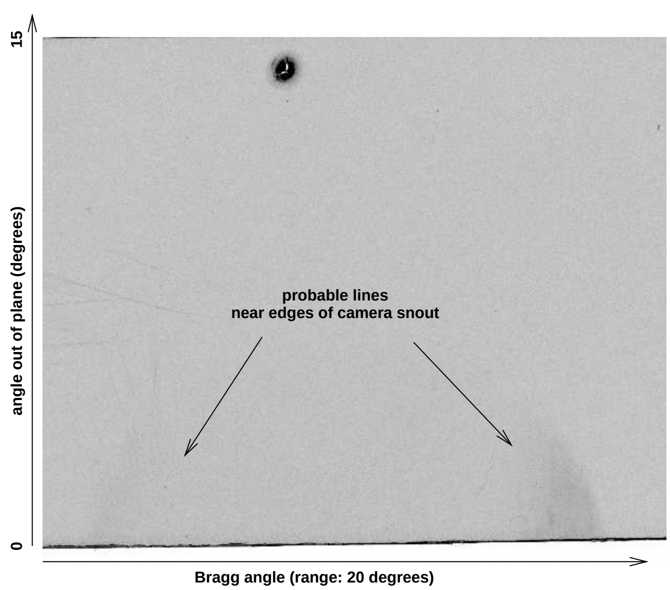

Figure 22: Time-integrated Laue diffraction record, shot 15002.

4.6 15004

Shot 15004 was another static test. The time-integrated Bragg record again showed a broad, curved line with a mottled intensity. The time-resolved Bragg record showed two apparent lines, plus other structures. This behavior can indicate a damaged photocathode; the photocathode was changed after this shot. A trial was performed of an image plate x-ray detector. This obscured the film cassette and x-ray streak camera to the Laue side of the sample. (Figs 23 and 24.)

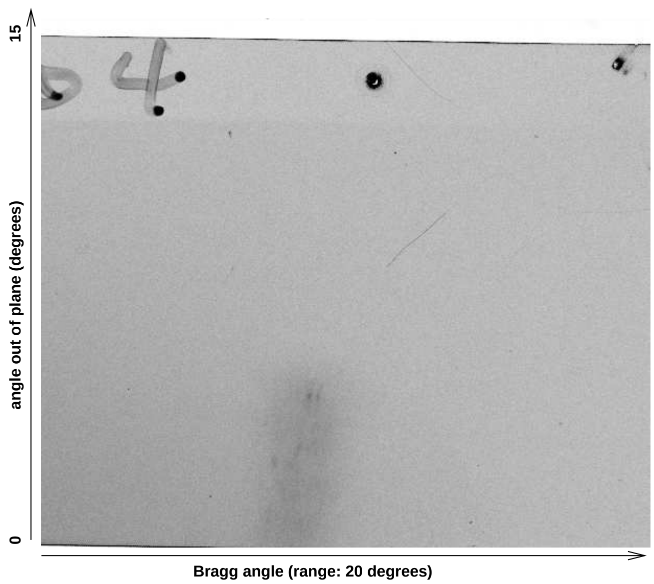

Figure 23: Time-integrated Bragg diffraction record, shot 15004.

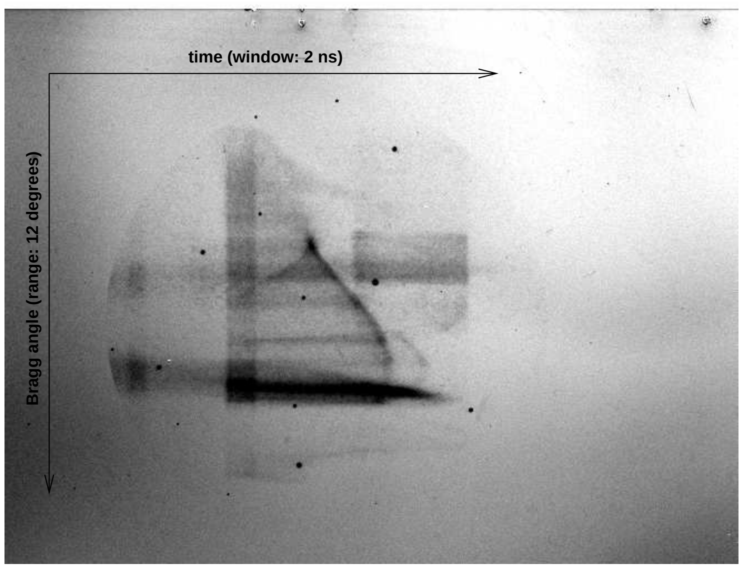

Figure 24: Time-resolved Bragg diffraction record, shot 15004.

4.7 15009

In shot 15009, the time-integrated Bragg record showed a broad, curved line. The time-resolved Bragg record showed two clear lines: one likely the unshocked signal; one fainter and likely from shocked material. There was no signal on the Laue detectors. (Figs 25 to 28.)

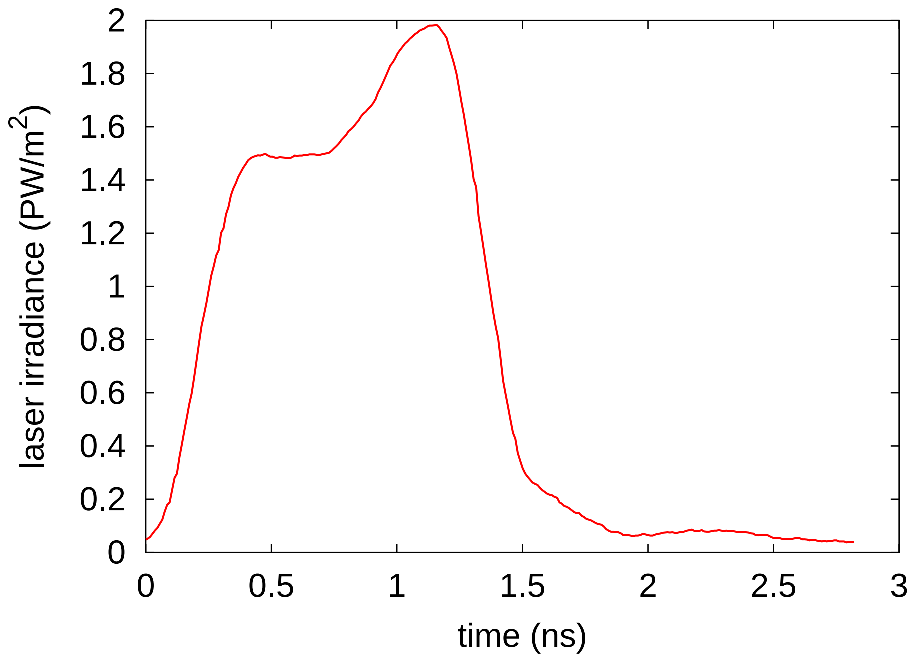

Figure 25: Laser irradiance history, shot 15009.

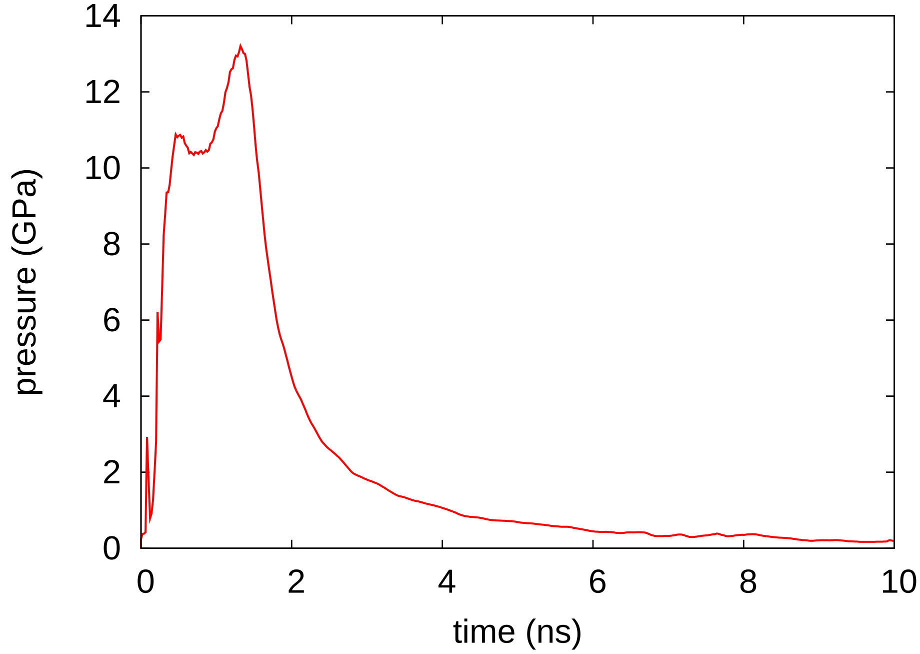

Figure 26: Drive pressure history predicted from radiation hydrodynamics simulations, shot 15009.

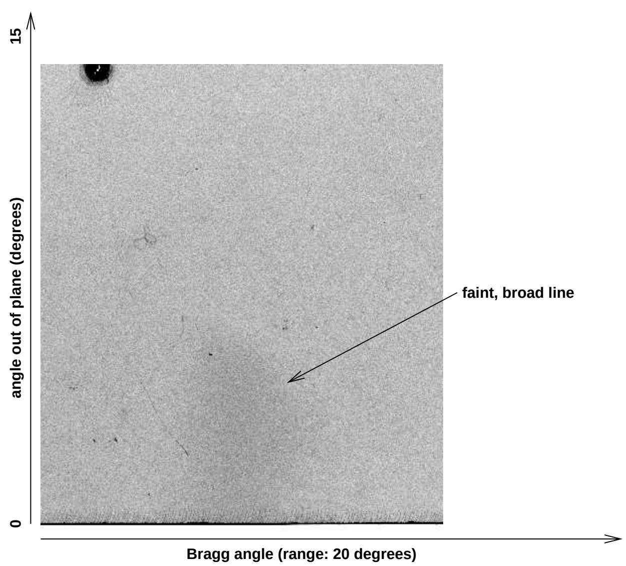

Figure 27: Time-integrated Bragg diffraction record, shot 15009.

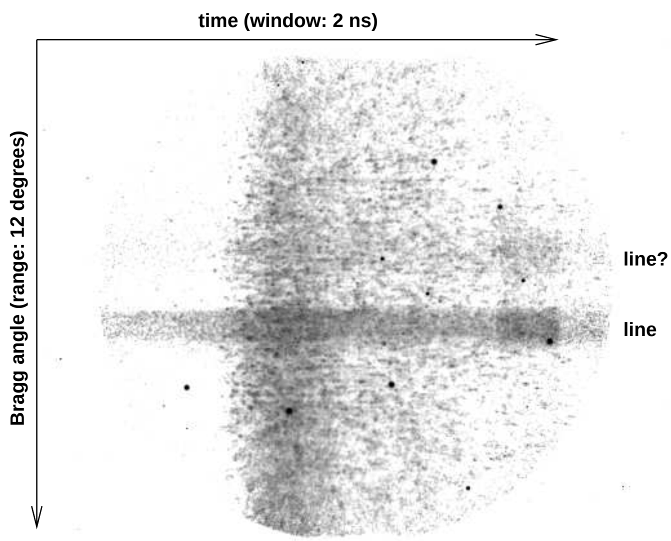

Figure 28: Time-resolved Bragg diffraction record, shot 15009.

4.8 15012

In shot 15012, the filtering was inadequate on the photodiode monitoring the drive beam, so the pulse shape record was saturated around its peak (registering zero in the drive history below). Simulations were performed using two drive histories: an idealized pulse based on the requested shape, and an energy scaling of the pulse obtained in shot 15009. The time-integrated Bragg record showed a broad, curved line. The time-resolved Bragg record showed two clear lines: either shocked and unshocked lines, or possibly another photocathode problem. The time-integrated Laue record was slightly exposed at the edges, suggesting lines just out of the field of view. There was no signal on the time-resolved Laue camera. (Figs 29 to 34.)

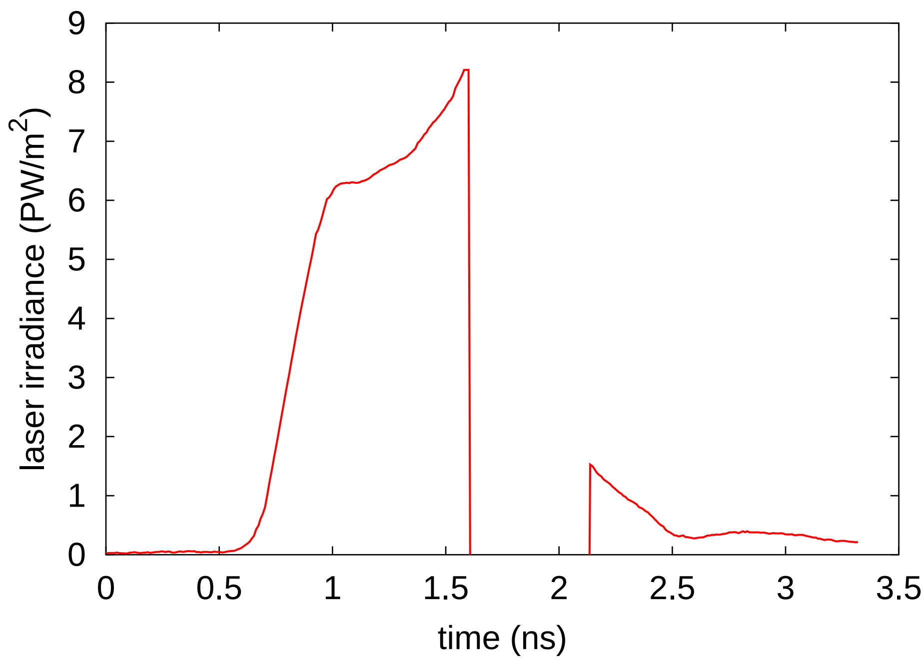

Figure 29: Laser irradiance history, shot 15012.

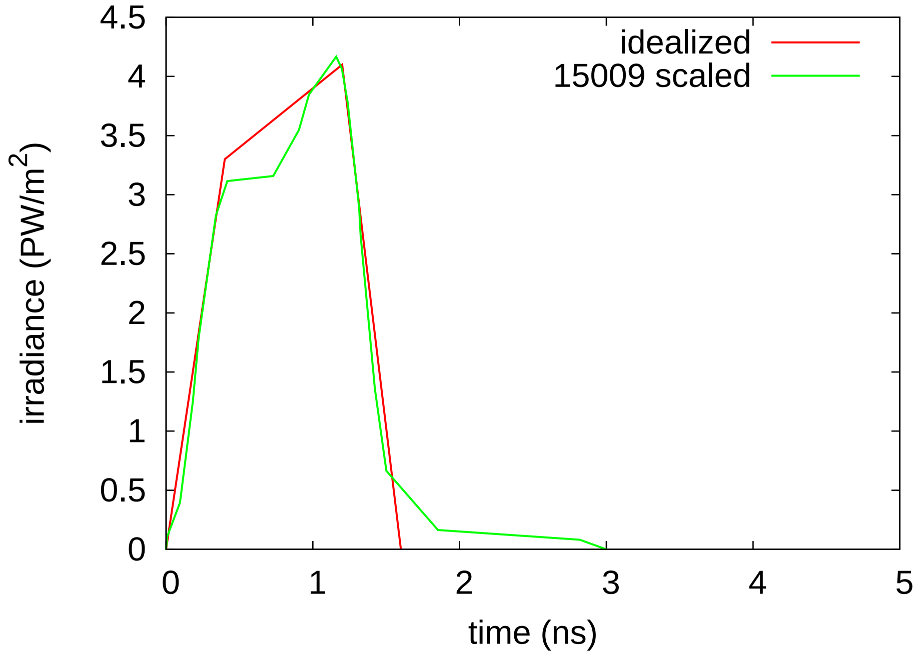

Figure 30: Laser irradiance history used for simulations of shot 15012.

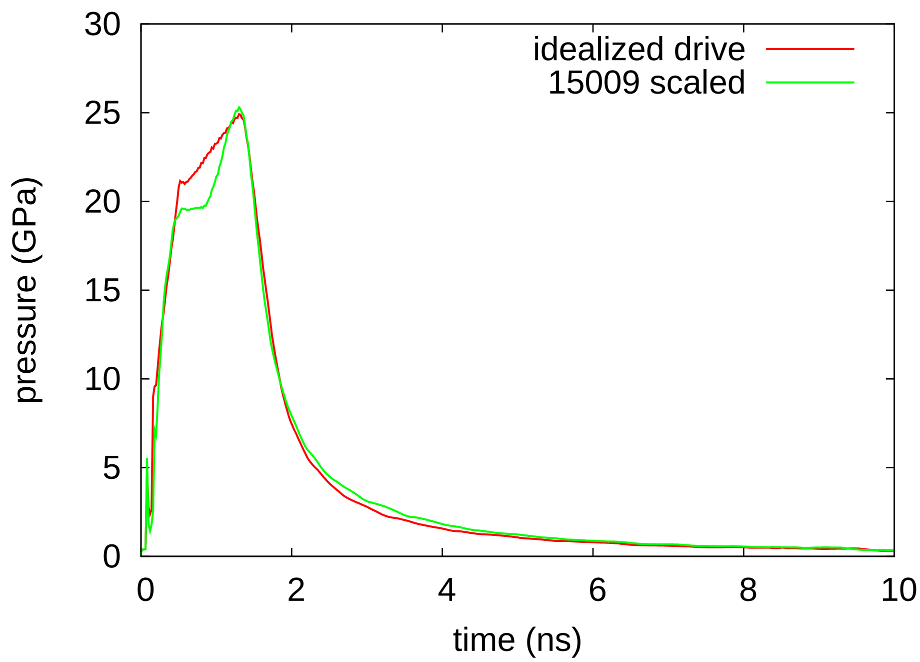

Figure 31: Drive pressure history predicted from radiation hydrodynamics simulations, shot 15012.

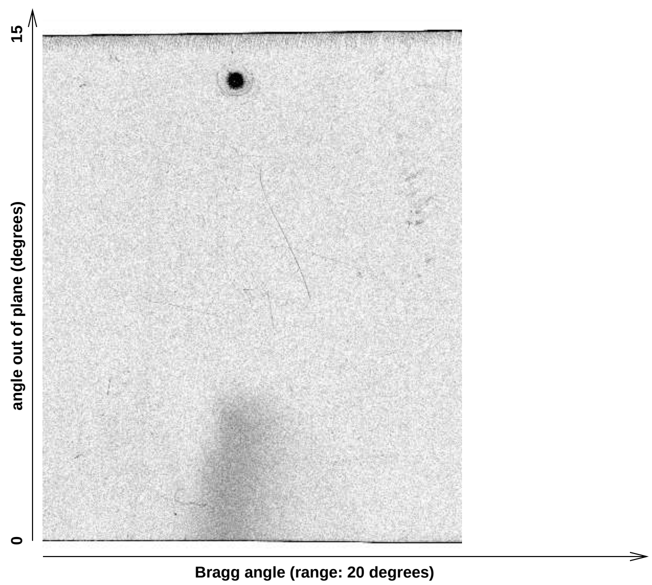

Figure 32: Time-integrated Bragg diffraction record, shot 15012.

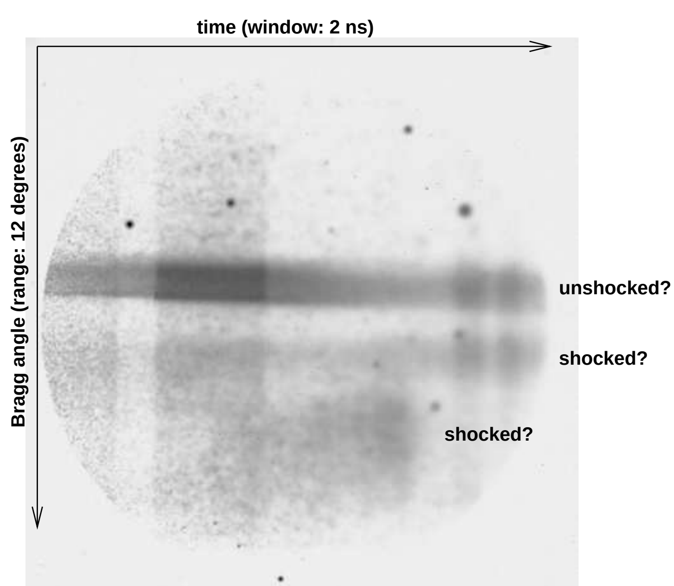

Figure 33: Time-resolved Bragg diffraction record, shot 15012.

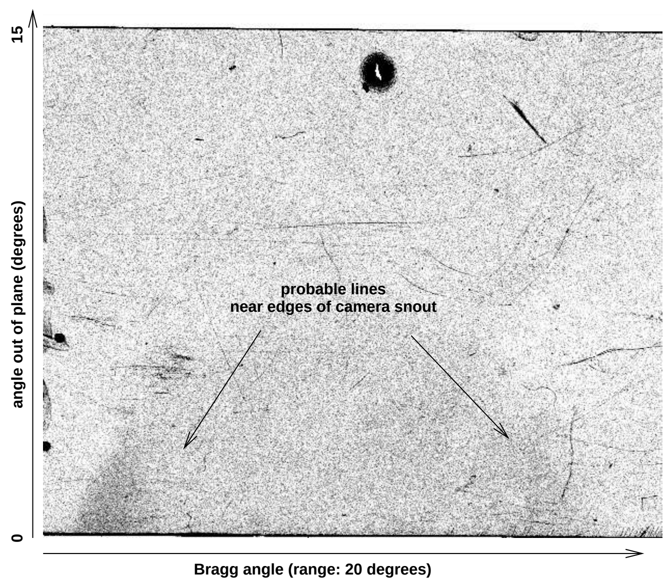

Figure 34: Time-integrated Laue diffraction record, shot 15012.

4.9 15014

In shot 15014, the time-integrated Bragg record showed faint signal lines toward the edges. The time-resolved Bragg record showed two clear lines: again, either shocked and unshocked lines, or possibly a photocathode problem. The time-integrated Laue record was exposed at a roughly uniform level. There was no signal on the time-resolved Laue camera. (Figs 35 to 38.)

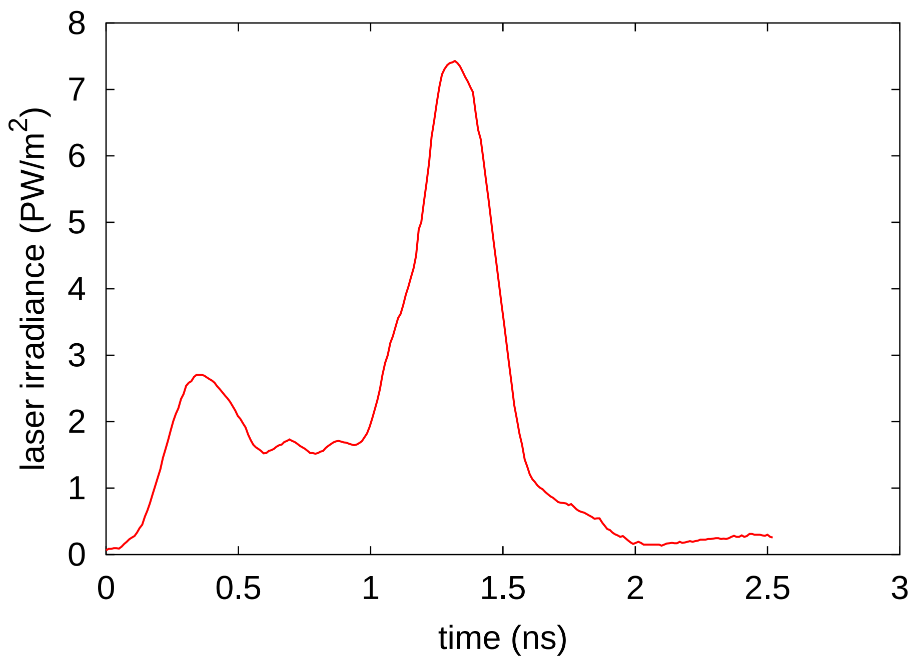

Figure 35: Laser irradiance history, shot 15014.

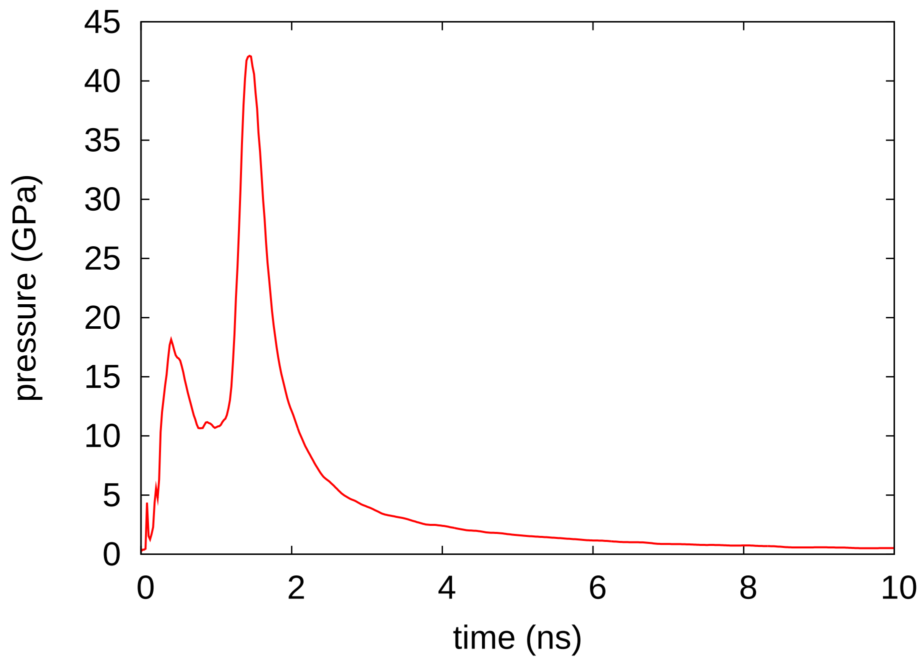

Figure 36: Drive pressure history predicted from radiation hydrodynamics simulations, shot 15014.

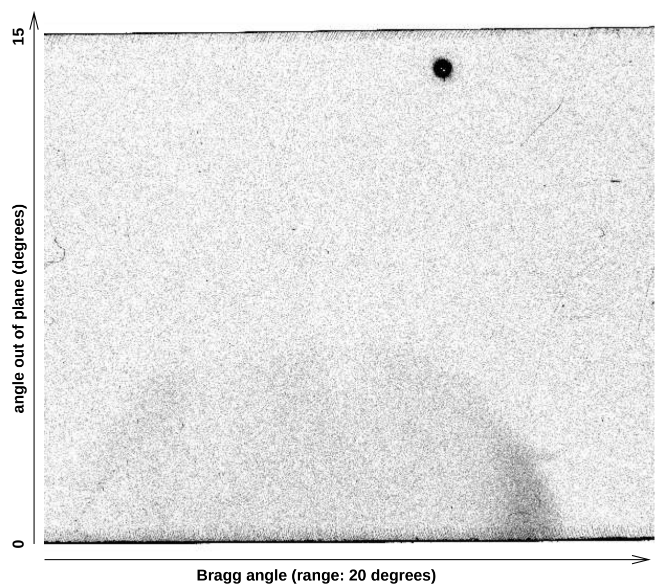

Figure 37: Time-integrated Bragg diffraction record, shot 15014.

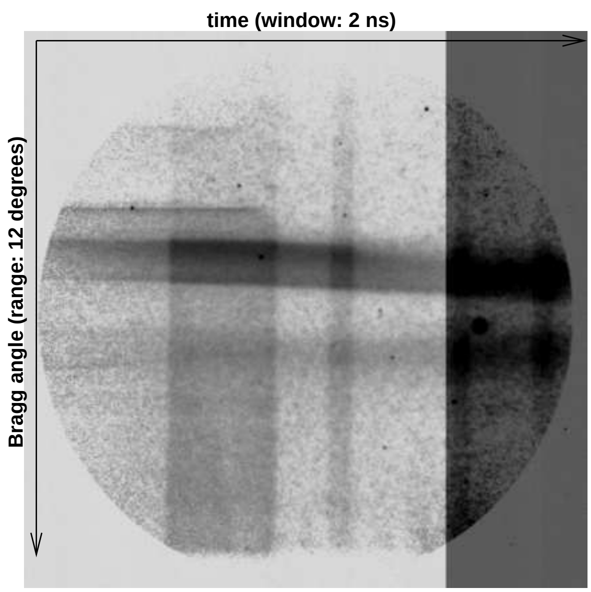

Figure 38: Time-resolved Bragg diffraction record, shot 15014.

4.10 15024

In shot 15024, an image plate was positioned in front of the Laue detectors. The time-integrated Bragg record was uniformly exposed, with no sign of diffraction lines. toward the edges. The time-resolved Bragg record showed two clear lines: again, either shocked and unshocked lines, or possibly a photocathode problem. There was no signal on the Laue detectors. (Figs 39 and 41.)

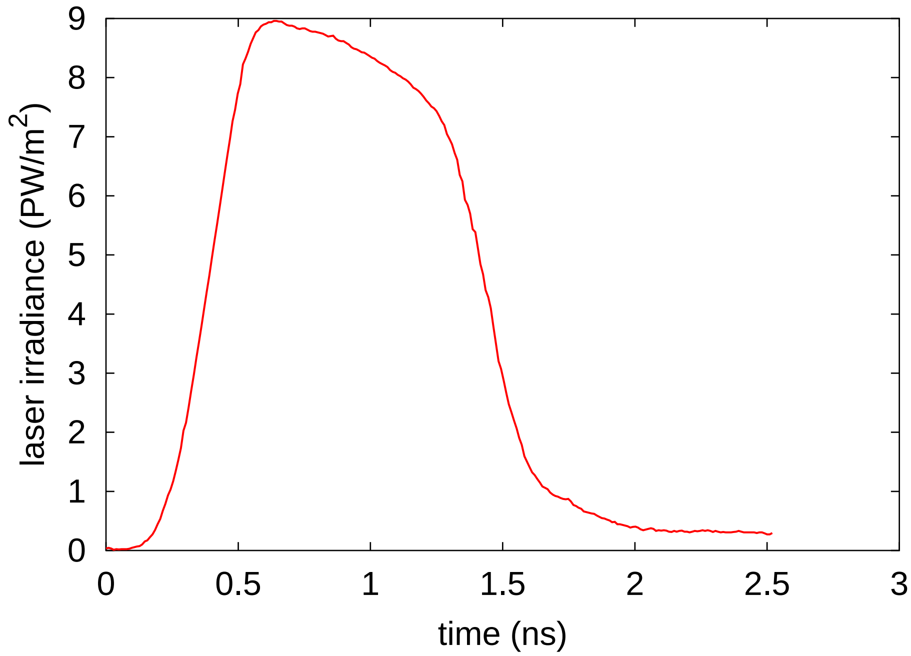

Figure 39: Laser irradiance history, shot 15024.

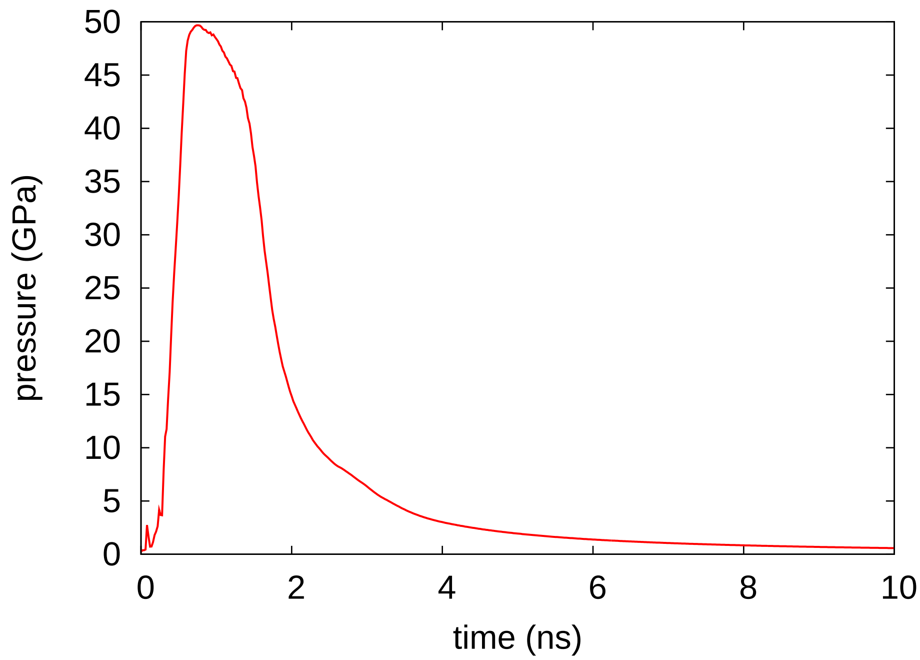

Figure 40: Drive pressure history predicted from radiation hydrodynamics simulations, shot 15024.

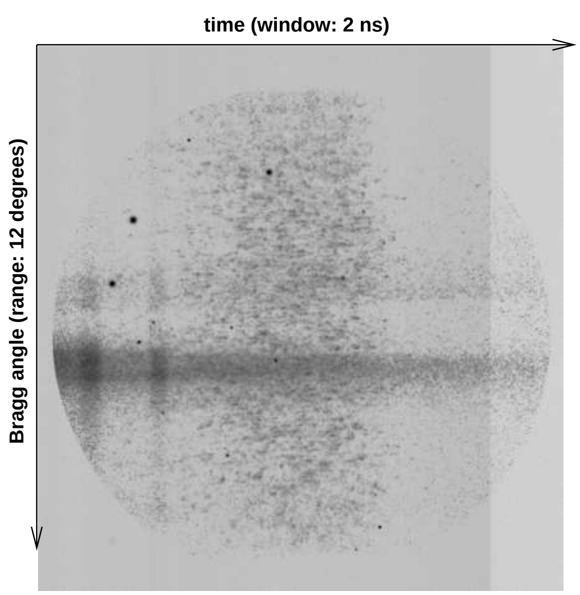

Figure 41: Time-resolved Bragg diffraction record, shot 15024.

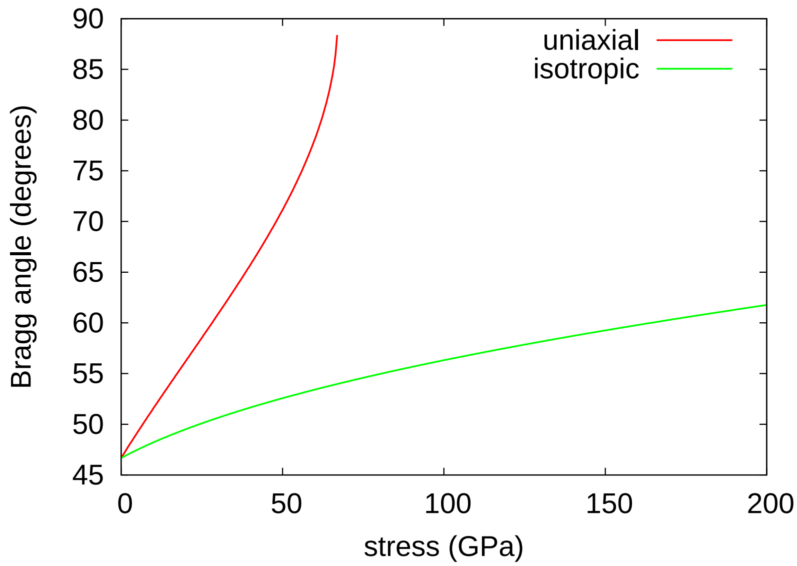

Figure 42: Dependence of (0002) Bragg angle in beryllium on shock pressure, for limiting assumptions about the deformation symmetry of the lattice.

5 Discussion

The interpretation of a single diffraction line in the absence of other data depends on the assumed orientation of the plane with respect to the shock, and on the assumed symmetry of deformation of the lattice. The extreme cases of lattice deformation are pure uniaxial or pure isotropic, and this assumption leads to significant differences in the compression or stress inferred from a given change in diffraction angle (Fig. 42).

Pure uniaxial lattice deformation occurs in elastic waves only; pure isotropic deformation occurs when the flow stress is negligible. When the drive pressure is not high enough to overdrive the elastic precursor, the diffraction signal would in principle consist of uniaxial compression to the elastic strain corresponding to the flow stress, and partially-isotropic compression to the highest pressure. Plastic flow acts to return the elastic strain to the flow stress, so the high pressure state generally includes a uniaxial component of this magnitude rather than pure isotropic compression. (The isotropic stress state is generally not an isotropic strain state for a single crystal, as the elastic constants generally vary with orientation.) When the drive pressure is high enough to overdrive the elastic wave, the high-pressure state is of course all that would be observed. If the elastic wave reaches an impedance mismatch at the opposite surface of the sample (e.g. and usually a free surface), it will reverberate between the surface and the plastic shock, creating regions of intermediate strain.

When interpreting time-resolved and time-integrated records, the detailed signal depends on the timing of the x-ray pulse with respect to the propagation of the different waves and the range of penetration of the x-rays in the sample. For beryllium, x-rays of the energy used here can penetrate hundreds of microns, so the diffraction signal was integrated over all positions through the thickness of the sample.

Continuum mechanics simulations were used to calculate the strain in the elastic precursor as a function of the flow stress.

The time-integrated Bragg records typically showed a clear arc centered in the film, consistent with diffraction from the (0002) planes. The arc was generally broader for shocked samples than in static tests, consistent with the measurement of compressed states. In some cases, a faint signal was evident corresponding to higher compressions. There were usually regions of stronger signal around the arc, presumably caused by diffraction from individual suitably-oriented grains.

The time-resolved Bragg records typically showed a strong doublet near the center, again presumably from (0002) planes. Most of the records showed a weaker line offset by around 2.5°, even for static tests.

This difference in angle does not correspond to any plausible planes, so it is most likely to reflect a fault in the x-ray streak camera, as was also indicated by examination of the photocathode. It is conceivable that in a rolled foil material would be present with a residual elastic strain, but the magnitude implied by this angle (~ 5 GPa) is too high to be plausible. In experiments with shock loading, the time-resolved Bragg records also showed a broad signal corresponding to lattice compression. The degree of compression can be converted to a uniaxial stress or an isotropic pressure by assuming a degree of uniaxiality. Assuming uniaxial strain around the [0001] direction, the range of angles in for example shot 15002 implied a flow stress in the range 3 to 8 GPa, which is consistent with values deduced from velocimetry. Assuming isotropic compression, the range of angles implied a shock pressure in the range 7 to 20 GPa, bracketing the expected shock pressure but with a much larger range than expected for any individual experiment. Unfortunately, the Bragg angles expected for uniaxial and isotropic compression in this range were fairly similar: the observed record is certainly a superposition of both types of deformation. This ambiguity should be absent in the higher-compression experiments needed to investigate shock-induced melting, as the Bragg angles would be significantly different and the elastic wave may be overdriven in many cases; a wider field of view would be needed to detect Bragg angles over the necessary range of compressions. The ambiguity would also be less in experiments on softer materials. In shot 15012, the shocked signal moved with time, possibly indicating lattice relaxation i.e. the transition from uniaxial to isotropic compression. The drive pressure was predicted to be relatively constant (compared with the change in lattice parameter); it seems possible that the signal has captured the decay of a very strong elastic precursor (~ 10 GPa) at early times.

The time-integrated Laue records typically showed two faint signals close to the edges of the field of view, i.e. around 15° apart. The position and spacing are consistent with the $\{10\bar{1}0\}$ and $\{11\bar{2}0\}$ lines at one edge and the $\{10\bar{1}1\}$ and $\{11\bar{2}1\}$ lines at the other. Presumably the {0002} lines did not appear – and the lines above did not appear on the Bragg record – because of the texture of the rolled foils. The position and low signal levels made it difficult to extract any useful distribution of angles.

6 Conclusions

Experiments were performed in which beryllium foils were loaded by laser ablation, and the distortion of the grains was monitored with *in situ* x-ray diffraction. X-ray powder patterns were clearly visible on the time-integrated (film) record positioned to capture reflections from {0002} planes, and there was evidence of lines at the edges of the opposite time-integrating record, consistent with diffraction from $\{10\bar{1}0\}$, $\{11\bar{2}0\}$, $\{10\bar{1}1\}$, and $\{11\bar{2}1\}$ planes. In some experiments, the x-ray streak cameras also recorded diffraction lines, but some apparent lines may have been caused by camera faults. The records clearly included signals from shocked and unshocked beryllium. The deviations in Bragg angle were consistent with strains anticipated from the ablative loading applied, and the range of flow stress deduced from surface velocimetry. In these initial experiments, the accuracy and separation of the changing diffraction lines was not sufficient to be used in isolation – velocimetry is essential, a wider angular coverage for x-ray detection is highly desirable, and camera faults should be eliminated before relying on polycrystal diffraction to obtain useful data. The technique does however show promise.

Acknowledgments

We would like to thank the TRIDENT staff, including Randy Johnson, Tom Hurry, Tom Ortiz, Fred Archuleta, Nathan Okamoto, and Ray Gonzales, for their hard work on the experiments. Bernie Carpenter (P-24) and Kathy Gallegos (Bechtel) scanned the films. Allan Hauer and Steve Batha provided funding through the Los Alamos program board of NNSA Campaign 10.

References

[1] A.V. Bushman, G.I. Kanel', A.L. Ni, and V.E. Fortov, *Intense Dynamic Loading of Condensed Matter* (Taylor and Francis, London, 1993).

[2] Q. Johnson, A. Mitchell, R.N. Keeler, and L. Evans, *X-ray diffraction during shock wave compression*, Phys. Rev. Lett. **25**, 1099 (1970).

[3] A. Loveridge, A. Allen, D. Kalantar, B. Remington, R.W. Lee, S. Weber, A. Hauer, G. Kyrala, D. Paisley, B. Holian, P. Lomdahl, T. Boehly, M.A. Meyers, D.C. Swift, J.S. Wark, *Anomalous response of silicon to uniaxial shock compression on nanosecond timescales*, Phys. Rev. Lett. **86**, 2349 (2001).

[4] P.A. Rigg and Y.M. Gupta, *Multiple x-ray diffraction to determine transverse and longitudinal lattice deformation in shocked lithium fluoride*, Phys. Rev. B **63**, 9, 094112 (2001).

[5] D.C. Swift, G.J. Ackland, A. Hauer, and G.A. Kyrala, *First principles equations of state for simulations of shock waves in silicon*, Phys. Rev. B **64**, 214107 (2001).

[6] D.C. Swift, D.L. Paisley, G.A. Kyrala and A. Hauer, *Simultaneous VISAR and TXD measurements on shocks in beryllium crystals*, Proc APS Topical Conference on Shock Compression of Condensed Matter, held Atlanta, GA, 25-29 Jun 2001; AIP CP620 (2002).

[7] D.C. Wilson et al, *The development and advantages of beryllium capsules for the National Ignition Facility*, Phys. Plasmas **5**, 5, pp 1953-9 (1998).

[8] P.A. Bradley and D.C. Wilson, *Physics of one-dimensional capsule designs for the National Ignition Facility*, Phys. Plasmas **6**, 11, pp 4293-303 (1999).

[9] J.D. Lindl, *Inertial confinement fusion* (Springer-Verlag, New York, 1998).

[10] D.C. Swift, T.E. Tierney IV, R.A. Kopp, and J.T. Gammel, *Shock pressures induced in condensed matter by laser ablation*, Phys. Rev. E **69**, 036406 (2004).

[11] D.C. Swift, J.T. Gammel, and S.M. Clegg, *Treatment of compounds and alloys in radiation hydrodynamics simulations of ablative laser loading*, Phys. Rev. E **69**, 056401 (2004).

[12] D.C. Swift, *TRIDENT Postshot Report: TXD Experiments, July - August 2001*, Los Alamos National Laboratory report LA-UR-01-5588 (2001).

[13] D.C. Swift, *TRIDENT materials shots ('Flying Pig 2'), August 2002*, Los Alamos National Laboratory report LA-UR-04-1475 (2004).

[14] D.C. Swift, *Laser-induced shock experiments on beryllium foils*, Los Alamos National Laboratory report LA-UR-01-6430 (2001).

[15] D.C. Swift, *Simulations of ablatively-driven shock wave experiments on beryllium (TRIDENT experiments: July-August 2000)*, Los Alamos National Laboratory report LA-UR-04-7411 (2004).

[16] G.B. Zimmermann and W.L. Kruer, Comments Plas. Phys. **2** 2, 51 (1975).

[17] Documentation for HYADES computer program, version 01.05.11 (Cascade Applied Sciences Inc, Golden, Colorado, 1998).

[18] S.P. Lyon and J.D. Johnson (Los Alamos National Laboratory), private communications on SESAME database (1998).

[19] Ya.B. Zel'dovich and Yu.P. Raizer, *Physics of shock waves and high temperature hydrodynamic phenomena*, (Academic Press, New York, 1966).

[20] R. Dendy, *Plasma Physics*, (Cambridge University Press, Cambridge, 1993).

[21] Documentation for LAGC1D computer program, version 5.2 (incorporating ARIADNE material properties library, version 7.0, and C++ mathematical class library, version 2.0), (Wessex Scientific and Technical Services Ltd, Perth, Scotland, 2003; `http://www.wxres.com`).